SolarPACES 2024, 30th International Conference on Concentrating Solar Power, Thermal, and Chemical Energy Systems

Receivers and Heat Transfer Media and Transport: Point Focus Systems

https://doi.org/10.52825/solarpaces.v3i.2306

© Authors. This work is licensed under a Creative Commons Attribution 4.0 International License

Published: 27 Aug. 2025

Techno-Economic Optimization of Falling Particle Receivers for Solar Tower Plants

Filip Sobic[1,*], Giancarlo Gentile[1], Marco Binotti[1], Andrea Giostri[1], and Giampaolo Manzolini[1]

[1]Politecnico di Milano, Italy

*Correspondence: Filip Sobic, filip.sobic@polimi.it

Abstract. Solid particle receivers are proposed as the next generation of receivers for solar tower CSP plants as they are able to overcome the temperature limits of solar salts. However, maximizing their performance requires robust design optimization tools. Therefore, this study proposes a methodology for the techno-economic optimization of the design of falling particle receivers for polar-field solar tower CSP plants. Given a specific solar field and location, the optimized design is derived using a parametric approach based on Levelized Cost of Electricity (LCOE) minimization, varying the height and the width of the receiver, as well as, the size of thermal energy storage. Methodology is applied to a 100 MW_{th} solar tower plant in Daggett, California, and the results show that the receiver sized using the proposed approach can achieve LCOE of 80.1 $/MWh that is by 2.2 % lower compared to the LCOE of the receiver sized only through on-design performance maximization.

Keywords: Particle Receiver, Solar Tower, Concentrated Solar Power, Techno-Economic Analysis

1. Introduction

The state-of-the-art solar tower technology adopts a surrounded heliostat field with an external cylindrical tubular receiver using solar salts as heat transfer fluid (HTF) coupled with a steam Rankine cycle [1]. However, the thermal stability issues of solar salts limit their maximum operating temperature up to 565°C [2], [3], thus limiting the efficiency of the power block (PB). Therefore, solid particles were proposed as an alternative HTF [1] that could provide temperatures over 700°C that allow supercritical CO_2 (sCO_2) Brayton cycle to achieve efficiencies over 50 % [4].

To fully exploit the advantages provided by this next generation of high temperature particle receivers, it is necessary to have tools for evaluating the optimal design of the receiver to be installed within a CSP plant. Therefore, the work presented here proposes a novel methodology for optimal sizing of falling particle receivers for polar-field solar tower plants, where the optimal size is identified by the minimum Levelized Cost of Electricity (LCOE). The proposed procedure evaluates the optimal design of the falling particle receiver optimizing both the height and the width, extending the works present in literature that consider only the area with aspect ratio equal to one, thereby providing insight into the impact of receiver aspect ratio on the overall plant performance. In addition to the receiver size, also the size of the thermal energy storage (TES) is considered in the optimization procedure. The required inputs include plant location with corresponding weather data, the solar field characteristics, as well as, PB technology and its performance map.

2. Methodology

The first step is to generate the solar field, using the open-source software SolarPILOT [5], considering a receiver size that results in image intercept efficiency similar to that of a conventional plant, while respecting the peak heat flux limit of the receiver. This receiver, used for solar field sizing, is referred to as the average receiver in this work. Since image size priority [5] is adopted as the aiming strategy, it is necessary to determine, for every combination of receiver height and width, the values of image offsets from the receiver edge that maximize the optical efficiency, while taking into account the limit on the peak heat flux. Furthermore, to reduce the computational burden, a yearly optical efficiency map for each receiver size is obtained from the map of the average receiver by scaling it with the ratio of design optical efficiency of the considered and average receiver. The following step is the evaluation of the off-design receiver performance for each receiver size using the thermal model. Then, obtained off-design receiver performance curves are coupled with the models simulating the performance of PB, TES, and auxiliaries, to evaluate the yearly performance of the overall plant. Finally, taking as input results of the yearly analysis, the economic analysis is carried out to evaluate the LCOE of each considered receiver configuration.

2.1 Receiver Thermal Model

The receiver thermal model used for evaluating the performance of the falling particle receiver is taken from previous work [6], and it is an improved version of the model developed in [7]. It simulates the performance of a falling particle receiver consisting of a cavity and a free-falling particle curtain that can exchange energy both with the ambient and the back wall of the cavity. Particle curtain is discretized in a finite number of control volumes, evaluating particle properties in both vertical and horizontal directions. Meanwhile, the back wall is discretized in all the three directions, evaluating its properties also along the thickness. The above-described discretization can be visualized in *Figure 1*.

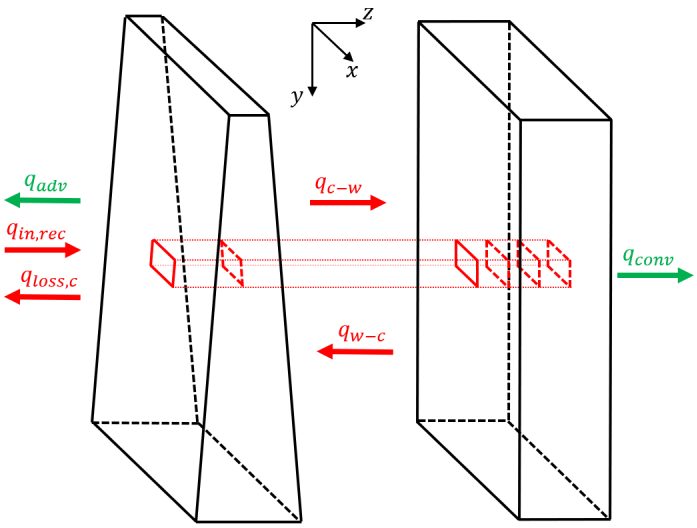

Figure 1. *Particle curtain and back wall discretization*

Volume fraction, velocity, and temperature distribution of the particle curtain are obtained by solving its mass balance, momentum balance, and energy balance that are reported in Eq. (1)-(3), while the back wall is described only using its energy balance. Even though it is not explicitly seen in mass and momentum balance equations, dependence on horizontal direction comes from the properties that depend on temperature which is not uniform along the horizontal direction due to non-uniform 2D heat flux.

$$\frac{d\dot{m}'_p}{dy} = 0 \tag{1}$$

$$\frac{d(\dot{m}'_p v_p)}{dy} = \varphi_p t_c \rho_p \left[g - \frac{18}{d_p^2} \frac{\rho_{air}}{\rho_p} \frac{\mu_{air,f}}{\rho_{air,f}} \cdot \left(1 + 0.40 Re_f^{\frac{2}{3}} \right) \cdot \left(v_p - v_{air} \right) \right] \tag{2}$$

$$-q_{abs,c} + q_{in,rec} - q_{loss,c} - q_{c-w} + q_{w-c} - q_{adv} = 0 \tag{3}$$

Where $\dot{m}'_p$ is lineic particle mass flow rate, v_p is particle velocity, φ_p is particle curtain volume fraction, t_c is curtain thickness, ρ_p is particle density, g is gravitational acceleration, d_p is particle diameter, ρ_{air} is the air density at ambient temperature, v_{air} is air velocity, $\mu_{air,f}$, $\rho_{air,f}$ and Re_f are dynamic viscosity, density, and Reynolds number of air at the local film temperature that is evaluated as the average of the particle temperature in the considered control volume and temperature of the ambient air. In Eq. (3), $q_{in,rec}$ denotes the non-uniform 2D heat flux reflected by the solar field and incident on the receiver, $q_{loss,c}$ is the radiative flux loss from the front part of the curtain. Meanwhile, q_{c-w} and q_{w-c} represent radiative fluxes going from the curtain to the wall and vice versa. Finally, q_{adv} is the advection flux from the curtain to the ambient air. Please note that every term in Eq. (3) is defined for every control volume of the particle curtain, and that, just for the sake of simplicity, control volume indices are omitted. These terms, together with q_{conv} that represents convection loss from the back wall to the ambient, are shown in ***Figure 1***, where red terms represent radiation heat transfer, while green ones represent all the others (for simplicity conduction heat transfer in the back wall is not represented).

2.2 Power Block Modelling

This work adopts the sCO_2 power cycle because it was selected by DOE as the most promising one for achieving the SunShot cost target [1]. The recompression cycle layout for the sCO_2 cycle is selected as it is able to mitigate the effect of different heat capacities on the cold and hot side of the recuperator. This is done by splitting the low-pressure stream after leaving the low-temperature recuperator and compressing it in a separate compressor before it joins the main stream at the inlet of the high-temperature recuperator, thus having different mass flow rates on the hot and cold side of the low-temperature recuperator [8]. Properties of CO_2 are evaluated using Span and Wagner [9] equation of state and the power block is modeled in ASPEN Plus.

2.3 Thermal Energy Storage and Auxiliaries

Two storage bins are adopted to store the hot and cold particles, respectively. Following the approach from [10], TES is modeled as a cylindrical containment having an aspect ratio (ratio of height over the diameter) of two. Therefore, TES dimensions for both bins are determined from the volume that is calculated using Eq. (4).

$$V_{TES,hot/cold} = \frac{\dot{Q}_{PB,in}^{nom} h_{TES} (1+\delta)}{\rho_{TES,hot/cold} \bar{c}_{p,TES} (T_{hot} - T_{cold})} \tag{4}$$

As can be seen, the volume of the stored media depends on the maximum amount of energy that can be stored in TES (capacity of TES), calculated by multiplying the hours of storage (h_{TES}) times the nominal thermal input to the PB ($\dot{Q}_{PB,in}^{nom}$), on the density of the storage medium, its specific heat capacity, and the difference between T_{hot} and T_{cold}, that are temperatures of the storage medium in hot and cold storage tank, respectively. The residual volume of storage above the maximum storage medium level in the bins is taken into account through parameter δ.

The electricity consumption of the particle elevator required to lift the cold particles coming from the cold storage bin to the receiver that sits at the top of the tower is evaluated using the approach proposed in [7]. Furthermore, auxiliary consumption of the plant itself consists of electricity consumption required to run the heliostat field, and baseline auxiliaries that are considered to occur over each hour during the year and evaluated as suggested in [11].

2.4 Yearly Performance and Economic Analyses

The yearly performance analysis is carried out on an hour-by-hour basis assessing the energy performance of the considered receiver configurations. As said before, to reduce the computational burden, the yearly optical efficiency map for each receiver size is derived from the yearly optical map of the average receiver using Eq. (5).

$$\eta_{opt}(\gamma, \theta_Z) = \eta_{opt}^{des} \frac{\eta_{opt}(\gamma, \theta_Z)}{\eta_{opt}^{des}}\Big|_{av} \quad (5)$$

Where η_{opt} is the optical efficiency of the solar field for a generic sun position, η_{opt}^{des} is the optical efficiency of the solar field at the on-design conditions, and the subscript av refers to the average receiver. Using this approach, it is possible to determine the incident solar energy on the receiver at each hour during the year, that, coupled together with receiver off-design performance curve gives the energy absorbed by the HTF at each hour. This energy is then sent either to the TES, PB, or both at the same time, depending on the amount of energy absorbed and plant status. For the sake of simplicity, the following operating principle is assumed for the PB: if the thermal energy provided by the HTF and TES is enough to run the PB at full load, then it is run at the full load, otherwise, PB is shut down.

Finally, it is necessary to carry out the economic analysis to be able to properly compare the performance of different receiver and TES sizes. Plant LCOE for every configuration is evaluated using the approach from [7]. Furthermore, cost functions used for evaluating costs of different components and values of adopted cost parameters are reported in Appendix.

3. Case Study

The proposed methodology is applied on a specific case study considering a plant located in Daggett, California (34.87 N, -116.89 W). The solar field is designed for a 100 MW_{th} receiver having the size resulting in image intercept efficiency similar to Gemasolar-like plant, taken from [12] and equal to 95.5 %. Moreover, it is necessary to consider the peak heat flux limit on the receiver that is selected equal to 2 MW/m^2 [6]. Solar field, receiver, and general design parameters, as well as, ranges of optimization variables (receiver height and width, and TES size), are reported in *Table 1*.

Table 1. *Solar field, receiver, and general design parameters, as well as, optimization variable ranges, adopted in the case study*

Solar field parameters	**Value**	**References**
Tower optical height	108 m	[13]
Sunshape model	Limb-darkened sun	[5]
Heliostat tracking error	0.00 mrad	[5]
Heliostat surface slope error	1.53 mrad	[5]
Reflective surface ratio	0.9583	[14]
Heliostat reflectivity	0.95	[14]
Soiling factor	0.95	[14]
Heliostat mirror area	115 m^2	[14]
Number of heliostats	1529	
Design sun position	Summer solstice	
Design DNI	1000 W/m^2	
Receiver parameters		
HTF inlet temperature	579 °C	
HTF outlet temperature	750 °C	
Particle diameter	$280 \cdot 10^{-6}$ m	[15]
Particle density	3300 kg/m^3	[15]
Particle absorptivity	0.906	[16]
Particle emissivity	0.754	[16]
Receiver height	8 – 16 m	
Receiver width	8 – 16 m	
General parameters		
TES capacity	4 – 12 h	
PB size	20 MW_{el}	
δ	0.1	[10]
Elevator efficiency	80 %	[7]
Heliostat field consumption	$5.22 \cdot 10^{-7}$ MW_{el}/m^2	[11]
Baseline auxiliaries	0.099 MW_{el}	[11]

Since the direct storage concept is adopted, same type of particles is used both as the HTF and as the storage medium. In particular, this work adopts CARBO Accucast ID 50 due to its high solar absorptivity [17] and durability [18]. Furthermore, size of the PB is fixed to 20 MW_{el} and its design ambient temperature is equal to 35°C, resulting in net electric efficiency of 46.6 %.

The cost of TES is evaluated as function of both the internal area and the temperature of particles stored inside, expressed in °C. The cost of all PB components is taken from [19], except for the primary heat exchanger, whose cost is set at 150 $\$/kW_{th}$, based on the US Department of Energy metric [20]. The Balance of Plant costs are calculated using the approach from [7], where they are assumed to be a percentage of PB costs, with this percentage adopted from the System Advisor Model [21]. A detailed summary of all the cost functions considered in this work is provided in ***Error! Reference source not found.***, while

Error! Reference source not found. outlines the cost parameters used within these functions. The sources for all cost assumptions are referenced directly within the tables.

Table 2. *Adopted cost functions*

Cost category	Value	References
Land	$c_{land}A_{land}$	[5]
Heliostat field	$(c_{heliostat} + c_{site\ improvement})A_{heliostat\ field}$	[5]
Receiver	$37400A_{rec}$	[7]
Tower	$3 \cdot 10^6 \cdot \exp(0.0113H_{tower})$	[5]
Particle elevator	$58.37H_{lift}\dot{m}_{HTF}$	[7]
Thermal energy storage	$c_{bin}\left(1 + 0.3\frac{T_{hot/cold} - 600}{400}\right)A_{bin}$	[10]
Storage medium inventory	$c_{storage\ medium}m_{stored}$	
Power block	From [19] and [20]	
Balance of Plant	$\left(\frac{c_{BOP}}{c_{PB}}\right)_{SAM} C_{PB}$	[7]

Table 3. *Adopted cost parameters*

Cost parameter	Value	References
c_{land}	2.47 \$/m^2	[5]
$c_{heliostat}$	75 \$/m^2	[22]
$c_{site\ improvement}$	10 \$/m^2	[22]
c_{bin}	1053 \$/m^2	[10]
$c_{storage\ medium}$	1.5 \$/kg	[1]
$c_{BOP,SAM}$	290 \$/kW$_{el}$	[21]
$c_{PB,SAM}$	1040 \$/kW$_{el}$	[21]
$r_{contingency}$	10 %	[7]
$r_{construction}$	9 %	[7]
$r_{discount}$	7 %	[7]
$r_{inflation}$	2.5 %	[7]
$N_{lifetime}$	30 years	[7]
$O\&M_{fixed}$	40 \$/kW/y	[7]
$O\&M_{variable}$	3 \$/MWh	[7]

4. Results

4.1 On-Design Results

Optical, thermal, and solar-to-thermal efficiency at on-design conditions for all considered receiver sizes are reported in *Figure 2*. Moreover, anticipating the results of the economic analysis, the optimal receiver size identified through LCOE minimization is indicated with a red cross. As can be seen in *Figure 2*, the optical efficiency of the receiver increases with receiver size, as larger receiver sizes result in higher intercept efficiency. However, larger receiver areas result also in higher thermal losses from the receiver to the ambient, thus thermal

efficiency decreases with receiver size. Therefore, the solar-to-thermal efficiency, being a product of optical and thermal efficiency, has a global optimum.

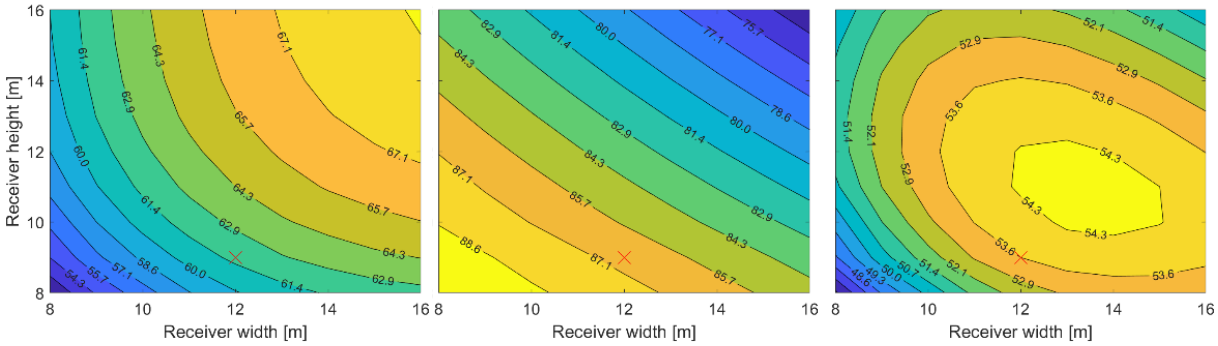

a) Design optical efficiency [%]

b) Design thermal efficiency [%]

c) Design solar-to-thermal efficiency [%]

Figure 2. *Falling particle receiver efficiencies at on-design conditions as function of the receiver size*

4.2 Yearly and Economic Analyses Results

Minimum LCOE over all the considered TES capacities for every combination of receiver height and width, with the corresponding yearly solar-to-thermal efficiency are reported in *Figure 3*. Again, as in the case of on-design conditions, solar-to-thermal efficiency has an optimum due to different trends of optical and thermal efficiencies. Furthermore, due to relatively low receiver cost, solar-to-thermal efficiency optimum drives the LCOE reduction: the optimal configuration from the economic point of view coincides with the one from the energy point of view.

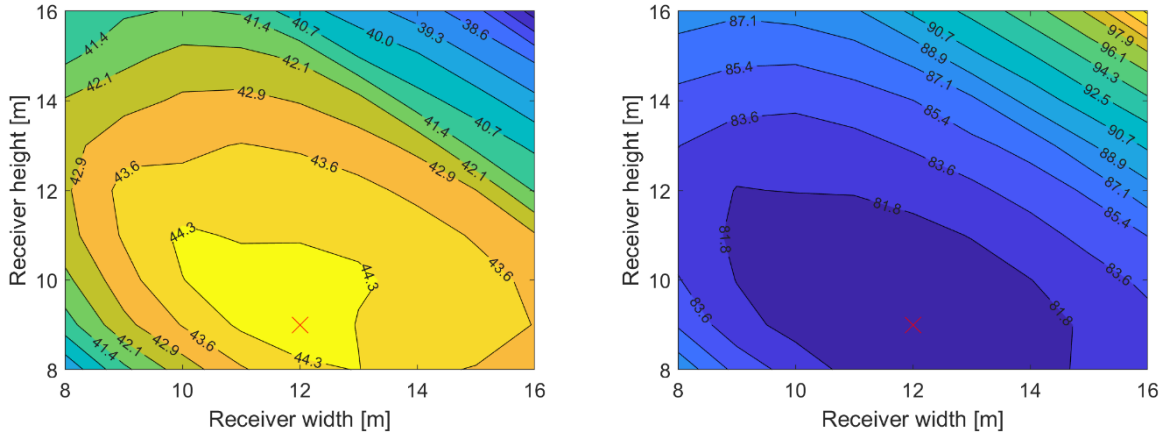

a) Yearly solar-to-thermal efficiency [%]

b) LCOE [$/MWh]

Figure 3. *Yearly solar-to-thermal efficiency and LCOE of the falling particle receiver as function of the receiver size*

However, it is interesting to note that the regions of high values of on-design and yearly solar-to-thermal efficiencies do not coincide completely. In the case of yearly solar-to-thermal efficiency, high efficiency region is moved towards smaller receiver sizes. This is explained by the fact that off-design thermal efficiency reduces significantly faster decreasing the thermal

input for larger sizes (see *Figure 4*), thus leading to yearly thermal efficiency that decreases much faster with receiver size with respect to the on-design one.

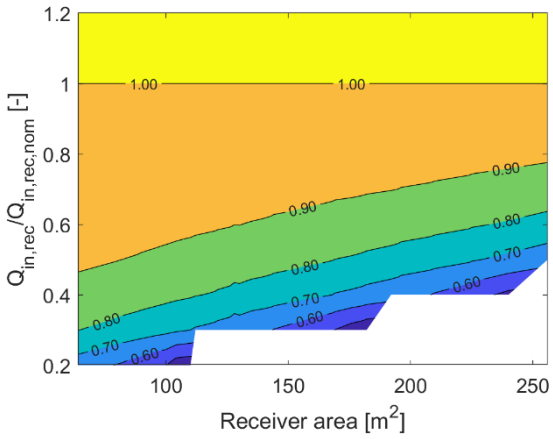

Figure 4. *Ratio between actual thermal efficiency and on-design thermal efficiency as a function of the falling particle receiver area and the normalized thermal input to the receiver*

Results of the falling particle receiver sizing using the proposed methodology (Yearly optimization) in terms of the optimal configuration (receiver heigh and width, and TES size), as well as, the on-design and yearly performance of the optimally sized receiver are reported in *Table 4*. Moreover, same results are also reported for the receiver sized using the simplified methodology (Design optimization), where the optimal size of the receiver is determined maximizing the on-design solar-to-thermal efficiency. As discussed already, optimum of on-design solar-to-thermal efficiency corresponds to higher area than that of the yearly one. Therefore, the on-design solar-to-thermal efficiency of the receiver sized using the simplified approach is higher due to the higher optical efficiency that overcomes the reduction of thermal efficiency. However, going to the yearly performance results, it is possible to see that difference in the yearly optical efficiency between the two designs is more or less constant (difference of 3.4 % for on-design vs 3.1 % for yearly), while the difference in the yearly thermal efficiency is much higher (5.0 %) compared to the difference in on-design thermal efficiency (3.0 %), due to reasons already discussed. Therefore, the proposed approach is able to provide LCOE that is lower by 2.2 % compared to the one obtained through the simplified sizing approach maximizing the on-design solar-to-thermal efficiency.

Table 4. *Comparison of optimal system configurations and performance metrics for receivers designed using the simplified (Design optimization) optimization approach and the proposed (Yearly optimization) optimization approach*

Optimal configuration	**Design optimization**	**Yearly optimization**
Receiver height [m]	11	9
Receiver width [m]	13	12
TES size [h]	8	8
On-design performance		
Optical efficiency [%]	65.2	61.8
Thermal efficiency [%]	83.7	86.7
Solar-to-thermal efficiency [%]	54.5	53.6
Yearly performance		
Optical efficiency [%]	59.3	56.2
Thermal efficiency [%]	74.5	79.5
Overall efficiency [%]	18.2	18.4
LCOE [$/MWh]	**81.9**	**80.1**

5. Conclusions

The developed methodology is a powerful tool for CSP industry and academic researchers as it allows to optimize the design of falling particle receivers taking into account optical and thermal performance, parasitic consumption for particle elevator, auxiliary consumption of the plant, and capital and operating costs. This methodology was applied to optimize the design of a 100 MW_{th} solar tower plant in Daggett (CA). Results show that the optima of on-design and yearly solar-to-thermal efficiencies diverge due to the more rapid decline in off-design thermal efficiency with increased receiver size. Therefore, adoption of the proposed methodology, that selects the receiver design and TES size through LCOE minimization, allowed for a LCOE reduction of 2.2 % compared to a simplified approach designing the receiver by maximizing the on-design solar-to-thermal efficiency. Moreover, the identified best design is characterized by aspect ratio of 0.75, showing the relevance of the proposed methodology, since aspect ratio equal to one (square receiver) is the common assumption present in literature.

Data availability statement

No data are available for this study..

Underlying and related material

There are no underlying or related materials associated with this work..

Author contributions

Filip Sobic: Conceptualization, Investigation, Methodology, Software, Visualization, Writing – Original Draft; **Giancarlo Gentile**: Conceptualization, Methodology, Writing – Review & Editing; **Marco Binotti**: Conceptualization, Writing – Review & Editing; **Andrea Giostri**: Conceptualization, Writing – Review & Editing; **Giampaolo Manzolini**: Conceptualization, Supervision, Writing – Review & Editing, Funding acquisition.

Competing interests

The authors declare that they have no competing interests.

References

[1] M. Mehos et al., “Concentrating Solar Power Gen3 Demonstration Roadmap,” NREL/TP--5500-67464, 1338899, Jan. 2017. doi: 10.2172/1338899.

[2] G. Gentile, G. Picotti, F. Casella, M. Binotti, M. E. Cholette, and G. Manzolini, “SolarReceiver2D: a Modelica Package for Dynamic Thermal Modelling of Central Receiver Systems,” IFAC-PapersOnLine, vol. 55, no. 20, pp. 259–264, 2022, doi: 10.1016/j.ifacol.2022.09.105.

[3] G. Gentile, G. Picotti, M. Binotti, M. E. Cholette, and G. Manzolini, “Dynamic thermal analysis and creep-fatigue lifetime assessment of solar tower external receivers,” Solar Energy, vol. 247, pp. 408–431, Nov. 2022, doi: 10.1016/j.solener.2022.10.010.

[4] F. Crespi, G. Gavagnin, D. Sánchez, and G. S. Martínez, “Supercritical carbon dioxide cycles for power generation: A review,” Applied Energy, vol. 195, pp. 152–183, Jun. 2017, doi: 10.1016/j.apenergy.2017.02.048.

[5] M. J. Wagner and T. Wendelin, “SolarPILOT: A power tower solar field layout and characterization tool,” Solar Energy, vol. 171, pp. 185–196, Sep. 2018, doi: 10.1016/j.solener.2018.06.063.

[6] O. Pasqualotto, F. Sobic, G. Gentile, M. Binotti, A. Giostri, and G. Manzolini, "A falling particle receiver thermal model for system-level analysis of solar tower plants," Solar Energy, vol. 268, p. 112117, Jan. 2024, doi: 10.1016/j.solener.2023.112117.
[7] L. F. González-Portillo, K. Albrecht, and C. K. Ho, "Techno-Economic Optimization of CSP Plants with Free-Falling Particle Receivers," Entropy, vol. 23, no. 1, p. 76, Jan. 2021, doi: 10.3390/e23010076.
[8] D. Alfani, M. Astolfi, M. Binotti, P. Silva, and E. Macchi, "Off-design performance of CSP plant based on supercritical CO2 cycles," presented at the SOLARPACES 2019: International Conference on Concentrating Solar Power and Chemical Energy Systems, Daegu, South Korea, 2020, p. 130001. doi: 10.1063/5.0029801.
[9] R. Span and W. Wagner, "A New Equation of State for Carbon Dioxide Covering the Fluid Region from the Triple-Point Temperature to 1100 K at Pressures up to 800 MPa," Journal of Physical and Chemical Reference Data, vol. 25, no. 6, pp. 1509–1596, Nov. 1996, doi: 10.1063/1.555991.
[10] R. Buck and S. Giuliano, "Impact of solar tower design parameters on sCO2-based solar tower plants," 2018, DuEPublico: Duisburg-Essen Publications Online, University of Duisburg-Essen, Germany. doi: 10.17185/DUEPUBLICO/46098.
[11] G. Kolb, "An evaluation of possible next-generation high temperature molten-salt power towers.," SAND2011-9320, 1035342, Dec. 2011. doi: 10.2172/1035342.
[12] F. Rinaldi, M. Binotti, A. Giostri, and G. Manzolini, "Comparison of Linear and Point Focus Collectors in Solar Power Plants," Energy Procedia, vol. 49, pp. 1491–1500, 2014, doi: 10.1016/j.egypro.2014.03.158.
[13] P. Falcone, "A handbook for solar central receiver design," SAND-86-8009, 6545992, ON: DE87009985, Dec. 1986. doi: 10.2172/6545992.
[14] G. Agsburger, "Thermo-economic optimisation of large solar tower power plants," Jan. 2013, doi: 10.5075/EPFL-THESIS-5648.
[15] C. K. Ho et al., "Performance Evaluation of a High-Temperature Falling Particle Receiver," in Volume 1: Biofuels, Hydrogen, Syngas, and Alternate Fuels; CHP and Hybrid Power and Energy Systems; Concentrating Solar Power; Energy Storage; Environmental, Economic, and Policy Considerations of Advanced Energy Systems; Geothermal, Ocean, and Emerging Energy Technologies; Photovoltaics; Posters; Solar Chemistry; Sustainable Building Energy Systems; Sustainable Infrastructure and Transportation; Thermodynamic Analysis of Energy Systems; Wind Energy Systems and Technologies, Charlotte, North Carolina, USA: American Society of Mechanical Engineers, Jun. 2016, p. V001T04A006. doi: 10.1115/ES2016-59238.
[16] A. Calderón et al., "Review of solid particle materials for heat transfer fluid and thermal energy storage in solar thermal power plants," Energy Storage, vol. 1, no. 4, p. e63, Aug. 2019, doi: 10.1002/est2.63.
[17] N. P. Siegel, M. D. Gross, and R. Coury, "The Development of Direct Absorption and Storage Media for Falling Particle Solar Central Receivers," Journal of Solar Energy Engineering, vol. 137, no. 4, p. 041003, Aug. 2015, doi: 10.1115/1.4030069.
[18] R. C. Knott, D. L. Sadowski, S. M. Jeter, S. I. Abdel-Khalik, H. A. Al-Ansary, and A. El-Leathy, "High Temperature Durability of Solid Particles for Use in Particle Heating Concentrator Solar Power Systems," in Volume 1: Combined Energy Cycles, CHP, CCHP, and Smart Grids; Concentrating Solar Power, Solar Thermochemistry and Thermal Energy Storage; Geothermal, Ocean, and Emerging Energy Technologies; Hydrogen Energy Technologies; Low/Zero Emission Power Plants and Carbon Sequestration; Photovoltaics; Wind Energy Systems and Technologies, Boston, Massachusetts, USA: American Society of Mechanical Engineers, Jun. 2014, p. V001T02A041. doi: 10.1115/ES2014-6586.
[19] N. T. Weiland, B. W. Lance, and S. R. Pidaparti, "sCO2 Power Cycle Component Cost Correlations From DOE Data Spanning Multiple Scales and Applications," in Volume 9: Oil and Gas Applications; Supercritical CO2 Power Cycles; Wind Energy, Phoenix, Arizona, USA: American Society of Mechanical Engineers, Jun. 2019, p. V009T38A008. doi: 10.1115/GT2019-90493.

[20] University of Adelaide et al., “Gen 3 Particle Pilot Plant (G3P3) -- High-Temperature Particle System for Concentrating Solar Power (Phases 1 and 2),” SAND2021-14614, 1832285, 701739, Nov. 2021. doi: 10.2172/1832285.

[21] N. Blair et al., “System Advisor Model (SAM) General Description (Version 2017.9.5),” Golden, CO: National Renewable Energy Laboratory, NREL/TP-6A20-70414. [Online]. Available: https://www.nrel.gov/docs/fy18osti/70414.pdf

[22] M. Mehos, C. Turchi, J. Jorgenson, P. Denholm, C. Ho, and K. Armijo, “On the Path to SunShot: Advancing Concentrating Solar Power Technology, Performance, and Dispatchability,” Golden, CO: National Renewable Energy Laboratory, NREL/TP-5500-65688, 2016. [Online]. Available: http://www.nrel.gov/docs/fy16osti/65688.pdf.